

## Single, double, and triple Auger decay of the Xe $4p$ core-hole states

Y. Hikosaka,<sup>1</sup> P. Lablanquie,<sup>2</sup> F. Penent,<sup>2</sup> T. Kaneyasu,<sup>1</sup> E. Shigemasa,<sup>1</sup> J. H. D. Eland,<sup>3</sup> T. Aoto,<sup>4</sup> and K. Ito<sup>4</sup>

<sup>1</sup>*UVSOR Facility, Institute for Molecular Science, Okazaki 444-8585, Japan*

<sup>2</sup>*LCP-MR, Université Pierre et Marie Curie-Paris 6 and CNRS (UMR 7614), 11 rue Pierre et Marie Curie, 75231 Paris Cedex 05, France*

<sup>3</sup>*Physical and Theoretical Chemistry Laboratory, South Parks Road, Oxford OX1 3QZ, United Kingdom*

<sup>4</sup>*Photon Factory, Institute of Materials Structure Science, Oho, Tsukuba 305-0801, Japan*

(Received 30 April 2007; published 13 September 2007)

Auger decay of Xe<sup>+</sup> states arising from  $4p$  ionization has been studied with a very efficient multielectron coincidence method. Coster-Kronig decay from Xe<sup>+</sup>  $4p^{-1}$  and the subsequent decay into Xe<sup>3+</sup> states with three valence holes are identified. Formation of Xe<sup>4+</sup> is also observed as quadruple coincidences between a  $4p$  photoelectron and three Auger electrons. The relative probabilities of individual multi-ionization processes are determined from the coincidence yields.

DOI: [10.1103/PhysRevA.76.032708](https://doi.org/10.1103/PhysRevA.76.032708)

PACS number(s): 32.80.Fb, 32.80.Hd

### I. INTRODUCTION

Inner-shell photoionization of atoms can produce a variety of multiply charged ions in energetically accessible states by simple multiple Auger transitions. The multi-ionization processes can be identified using ordinary Auger electron spectroscopy only when both the initial core-hole states and the attributions of the Auger lines are not ambiguous. However, the overlap of Auger lines from different core-holes and different multi-ionization steps often prevents a full interpretation of the Auger electron spectra. Observation in coincidence of electrons emitted in each multi-ionization process enables us to gain clear identifications of the process. Thanks to recent improvements in coincidence spectroscopic techniques, our understanding has been extended up to Auger processes forming triply charged ion states [1–5] and quadruply charged ion states [6,7].

In this work we have investigated Auger decay of Xe<sup>+</sup> states formed by  $4p$  ionization using a very efficient multielectron coincidence method. The independent particle model fails completely for these Xe<sup>+</sup>  $4p^{-1}$  states, due to the strong interaction with the  $4d^{-2}nf$  and  $4d^{-2}ef$  configuration [8]. An anomalous photoelectron peak structure thus appears in the  $4p$  photoelectron spectrum [9–12]: the expected  $4p_{1/2}$  photoelectron line is dissolved and no longer visible, while the  $4p_{3/2}$  structure consists of several fine components. We will use the notation “ $4p$ ”<sup>-1</sup> to represent this strongly correlated state which includes the  $4p_{3/2}^{-1}$  and  $4d^{-2}nf$  characters. The decay process of Xe<sup>+</sup> “ $4p$ ”<sup>-1</sup> has been studied by Auger electron spectroscopy [11,12] and by threshold electron-ion coincidence spectroscopy [13]. The Xe<sup>+</sup> “ $4p$ ”<sup>-1</sup> state decays preferentially via Coster-Kronig transitions into Xe<sup>2+</sup>  $4d^{-1}5l^{-1}$  [11,12], and the Xe<sup>2+</sup> states so formed with  $4d$  holes are expected to decay further into Xe<sup>3+</sup>. In practice, the formation of Xe<sup>3+</sup> ions is abundantly observed in coincidence with “ $4p$ ” threshold photoelectrons [13]. The same coincidence measurement also revealed formation of Xe<sup>4+</sup> in the “ $4p$ ” decay, and this quadruple ionization was interpreted as simultaneous double Auger decay from Xe<sup>+</sup> “ $4p$ ”<sup>-1</sup> followed by subsequent Auger decay [13].

In the present study we have used a magnetic-bottle-type electron spectrometer whose powerful capability in multi-

electron coincidence observations has recently been described and demonstrated [4–7,14,15]. The coincidence dataset we accumulated includes complete information on the energy correlations among the several electrons emitted, from which we have deduced extensive information on single, double, and triple Auger decay from Xe<sup>+</sup> “ $4p$ ”<sup>-1</sup>.

### II. EXPERIMENT

The experiment was performed on beamline BL-1C of the Photon Factory. Single bunch operation provided a 624 ns repetition period for the 200-ps-width light pulses. The pulsed light was monochromatized by a grazing incidence monochromator using a varied-line-spacing plane grating. A gas beam effusing from a 500- $\mu$ m inner-diameter needle crossed the light beam at a right angle. Emitted electrons were analyzed in energy by their time of flight in a magnetic bottle electron spectrometer. As the descriptions of the spectrometer and the data accumulation scheme are given elsewhere [5], only a brief account will be given here. A strong permanent magnet (NdBFe,  $\sim 0.7$  T) located close to the interaction region creates, with the inhomogeneous magnetic field, a magnetic mirror for electrons that are hence guided by the weak magnetic field ( $\sim 1$  mT) of a long solenoid toward a position sensitive detector composed of two micro-channel plates followed by a phosphor screen. Signals from the detector are fed into a multistart (common-stop) time-to-digital converter (RoentDek TDC8). The converter is triggered by the arrival of a first electron and is stopped, after a 10  $\mu$ s delay, by the ring clock signal. All the electrons arriving in this time window are detected. Their absolute time of flight is then recalculated with respect to the ring clock. Calibration for the conversion from the electron flight time to kinetic energy was first obtained by measuring He  $1s$  photoelectrons at different photon energies, and was then adjusted with the Xe  $4d$  Auger lines [16]. The energy resolution was estimated by measuring He  $1s$  photoelectrons at different photon energies. For electrons between 1 and 300 eV kinetic energy, the energy resolving power of the apparatus,  $E/\Delta E$ , was nearly constant at 50, while, for electrons of less than 1 eV,  $\Delta E$  was limited to 20 meV. Coincidence yields for two

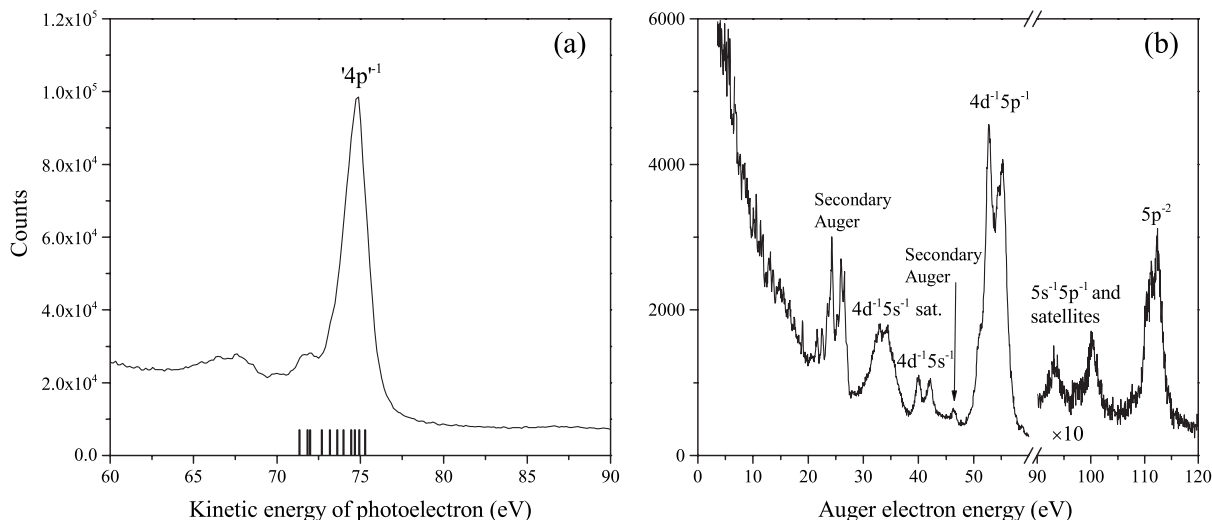


FIG. 1. (a) Xe “4*p*” photoelectron spectrum measured at a photon energy of 220.3 eV. The locations of the Xe<sup>+</sup> “4*p*”<sup>−1</sup> fine components observed in a higher resolution photoelectron spectrum [12] are indicated. (b) Xe “4*p*” Auger electron spectrum deduced from the coincidence dataset, where “4*p*” photoelectrons in the kinetic energy range of 70.5–77.8 eV are used for filtering the coincidence events relevant to the “4*p*” decay. The relative intensities of the Xe<sup>2+</sup> structures in Fig. 1(b) are listed in Table I.

photoelectrons associated with double photoionization of Ne were measured at different photon energies, with reference to the single photoionization yields. By comparing with reported ratios of single to double photoionization of Ne [17], it was estimated that the detection efficiency of the spectrometer was constant around 60% for electrons of less than 200 eV.

### III. RESULTS AND DISCUSSION

Multielectron coincidence spectroscopy was performed on Xe at a photon energy of 220.3 eV (i.e., about 75 eV above the “4*p*” threshold), where a coincidence dataset was accumulated for 20 hours with an average count rate of 1500 cps (counts per second). The photon bandwidth was set

to 0.15 eV. This photon energy was chosen in order to avoid overlap between the photoelectron and the Auger electrons. Figure 1(a) shows an electron spectrum in the kinetic energy range of 60–90 eV, which displays the “4*p*” photoelectron structure. The energy resolution for the photoelectrons is around 1.5 eV [full width at half-maximum (FWHM)], and thus the spectrum shows only the envelope of the fine components of Xe<sup>+</sup> “4*p*”<sup>−1</sup> [11,12]. The “4*p*” Auger electron spectrum deduced from the coincidence dataset is represented in Fig. 1(b), as observed in coincidence with photoelectrons selected in the kinetic energy range 70.5–77.8 eV. In the kinetic energy region 30–70 eV the Auger electron spectrum exhibits structures due to Coster-Kronig decay into Xe<sup>2+</sup> 4*d*<sup>−1</sup>5*l*<sup>−1</sup> states. In addition, weak structures due to the normal Auger decay forming two valence holes are discernible in the energy region 90–115 eV. The general features

TABLE I. Branching ratio for the decay of Xe<sup>+</sup> “4*p*” into Xe<sup>2+</sup>, estimated from the band intensities of the “4*p*” Auger electron spectrum in Fig. 1(a), and compared with multiconfigurational Dirac-Fock calculations including and excluding the final ionic state configuration interaction (FISCI) [11].

Decay from Xe <sup>+</sup> “4 <i>p</i> ” <sup>−1</sup>	Branching ratio	Calculation [11]	
		With FISCI	Without FISCI
Normal Auger decay into Xe <sup>2+</sup> (5 <i>s</i> 5 <i>p</i> ) <sup>−2</sup>	5 <i>p</i> <sup>−2</sup>	0.03	0.048
	(5 <i>s</i> 5 <i>p</i> ) <sup>−2</sup> at 100 eV Auger energy	0.01	0.01
	(5 <i>s</i> 5 <i>p</i> ) <sup>−2</sup> at 92 eV Auger energy	0.01	0.012
Coster-Kronig decay into Xe <sup>2+</sup> 4 <i>d</i> <sup>−1</sup> 5 <i>l</i> <sup>−1</sup>	4 <i>d</i> <sup>−1</sup> 5 <i>p</i> <sup>−1</sup>	0.66	0.594
	4 <i>d</i> <sup>−1</sup> 5 <i>s</i> <sup>−1</sup>	0.06	0.083
	4 <i>d</i> <sup>−1</sup> 5 <i>s</i> <sup>−1</sup> satellites	0.17	0.253
Other decay forming Xe <sup>4+</sup>	0.06		

agree with those of a previous Auger spectrum [11]. The relative intensities of the structures in Fig. 1(b) correspond to branching ratios of the  $\text{Xe}^+$  “ $4p$ ” $^{-1}$  decay. They are listed in Table I, in comparison with the values from multiconfigurational Dirac-Fock calculations including and excluding the final ionic state configuration interaction [11]. The experimental values agree well with the calculation including the final state configuration interaction, which implies that the configuration interaction is essential in the description of the  $\text{Xe}^+$  “ $4p$ ” $^{-1}$  decay. Note that valence double photoionization, besides the  $\text{Xe}^+$  “ $4p$ ” $^{-1}$  decay, can also contribute to the intensities in Fig. 1(b), when one of the photoelectrons has a kinetic energy in the range 70.5–77.8 eV. This contribution is estimated as less than 1% and does not affect the values listed in Table I significantly. The valence double photoionization background contribution was estimated by inspecting coincidences with electrons in kinetic energy ranges different from the “ $4p$ ” photoelectron range.

Since the Auger final  $\text{Xe}^{2+}$  states with two valence holes have binding energies lower than the  $\text{Xe}^{3+}$  threshold ( $64.09 \pm 0.04$  eV [4]), these  $\text{Xe}^{2+}$  states are stable except for fluorescence decay. By contrast, the Coster-Kronig final  $\text{Xe}^{2+}$  states may undergo a further decay into  $\text{Xe}^{3+}$  states by filling the remaining  $4d$  core holes. The energies of the relevant states are shown in Fig. 2 as an energy level diagram. The sequential double Auger process from  $\text{Xe}^+$  “ $4p$ ” $^{-1}$  appears as triple coincidences between a “ $4p$ ” photoelectron and the two Auger electrons. Figure 3 displays a two-dimensional (2D) map showing the energy correlations between the two Auger electrons included in the triple coincidences. Several islands of intense spots are seen on the 2D map, and they can be assigned to transitions from the  $\text{Xe}^{2+}$   $4d^{-1}5l^{-1}$  states into  $\text{Xe}^{3+}$  states with three valence holes. Except for the island corresponding to  $4d^{-1}5s^{-1}$  satellites  $\rightarrow 5p^{-3}$ , the fast and slow Auger electrons are emitted, respectively, on the first and second Auger decay from  $\text{Xe}^+$  “ $4p$ ” $^{-1}$ . From the coincidence counts on the 2D map, we can determine the branching ratios in the subsequent Auger decay from the Coster-Kronig final  $\text{Xe}^{2+}$  states. The branching ratios are summarized in Table II.

Besides the sequential double Auger decay observed as spots on the 2D map, direct double Auger decay is possible from  $\text{Xe}^+$  “ $4p$ ” $^{-1}$  into  $\text{Xe}^{3+}$ . In the direct double Auger processes, the available energies given by energy differences

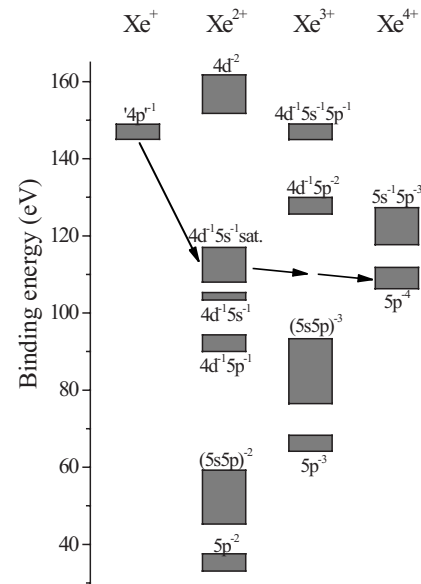


FIG. 2. Energy level diagram for  $\text{Xe}^+$ ,  $\text{Xe}^{2+}$ ,  $\text{Xe}^{3+}$ , and  $\text{Xe}^{4+}$  states. The arrows indicate the triple Auger process associated with the Coster-Kronig transition from  $\text{Xe}^+$  “ $4p$ ” $^{-1}$  to  $\text{Xe}^{2+}$   $4d^{-1}5s^{-1}$  satellites and subsequent double Auger decay of these  $\text{Xe}^{2+}$  states to  $\text{Xe}^{4+}$   $5p^{-4}$ .

between the  $\text{Xe}^+$  “ $4p$ ” $^{-1}$  and final  $\text{Xe}^{3+}$  states are continuously shared by the two Auger electrons. The corresponding electron yields, therefore, should appear as diagonal lines on the 2D map [4]. However, such structures are not discernible on this 2D map, which implies that direct double Auger processes are much less probable for the  $\text{Xe}^+$  “ $4p$ ” $^{-1}$  decay than the sequential ones. This is because the sequential process is associated with the dominating Coster-Kronig decay.

The spots in each island on the 2D map correspond to level-to-level correlations from  $\text{Xe}^{2+}$  to  $\text{Xe}^{3+}$ , and the spot intensities reflect the relative probabilities of the specific processes in the  $\text{Xe}^+$  “ $4p$ ” $^{-1}$  decay. Here we inspect more closely the level-to-level correlations from  $\text{Xe}^{2+}$  to  $\text{Xe}^{3+}$  only on the island corresponding to  $4d^{-1}5p^{-1} \rightarrow 5p^{-3}$  transitions, because the spots are well isolated from each other and the energy levels of the  $\text{Xe}^{2+}$  and  $\text{Xe}^{3+}$  states are well known. The coincidence yields are replotted in Fig. 4 as a function of binding energy of  $\text{Xe}^{2+}$  and that of  $\text{Xe}^{3+}$ .

TABLE II. Branching ratio for the decay of the  $\text{Xe}^{2+}$   $4d^{-1}5l^{-1}$  states, estimated from the coincidence yields on the two-dimensional map in Fig. 3(b).

$\text{Xe}^{2+}$ states	Total	Decay into $\text{Xe}^{3+}$				Double Auger to $\text{Xe}^{4+}$
		$5p^{-3}$	$5s^{-1}5p^{-2}$	$5s^{-1}5p^{-2}$ satellite	$5s^{-2}5p^{-1}$	
$4d^{-1}5p^{-1}$	0.66	0.19	0.13	0.34		
$4d^{-1}5s^{-1}$	0.06		0.04		0.02	
$4d^{-1}5s^{-1}$ satellites	0.17	0.05		0.05	0.04	0.03

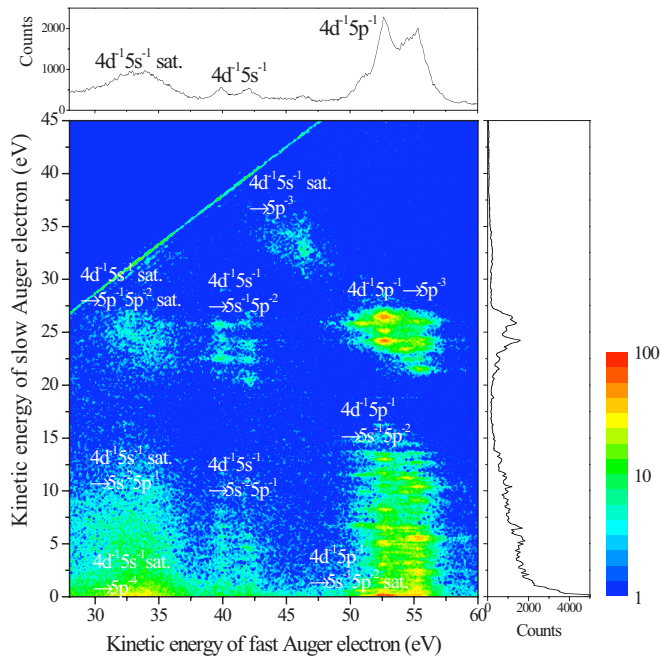


FIG. 3. (Color online) Energy correlation map between two Auger electrons emitted from  $\text{Xe}^+ 4p^{-1}$ . Coincidence yields are plotted on a log scale. The islands of intense spots are assigned to the transitions from Coster-Kronig final  $\text{Xe}^{2+}$  states into  $\text{Xe}^{3+}$  with three valence holes, as denoted on the map. Except for the island corresponding to  $4d^{-1}5s^{-1}$  satellites  $\rightarrow 5p^{-3}$ , the fast and slow Auger electrons are emitted, respectively, on the first and second steps of the  $\text{Xe}^+ 4p^{-1}$  Auger decay. Branching ratios in the subsequent Auger decay from the Coster-Kronig final  $\text{Xe}^{2+}$  states, which are determined from the coincidence counts on this map, are summarized in Table II. The top and right-hand panels show the projections of the coincidence yields onto the horizontal and vertical axes, respectively.

Here,

$$\begin{aligned} (\text{binding energies of } \text{Xe}^{2+}) &= (\text{photon energy}) \\ &\quad - (\text{photoelectron energy}) \\ &\quad - (\text{first Auger energy}) \end{aligned}$$

and

$$\begin{aligned} (\text{binding energies of } \text{Xe}^{3+}) &= (\text{binding energy of } \text{Xe}^{2+}) \\ &\quad - (\text{second Auger energy}). \end{aligned}$$

The energy levels of the  $\text{Xe}^{2+}$  [12] and  $\text{Xe}^{3+}$  states [4,18] are indicated in Fig. 4 with horizontal and vertical lines, respectively. The spots on the correlation map in Fig. 4 lie at the expected locations, though they extend diagonally because of the low-energy resolution for the fast “ $4p$ ” photoelectrons. The spot intensities correspond to the relative probabilities of the individual secondary Auger processes included in the  $\text{Xe}^+ 4p^{-1}$  decay. We see on the correlation map a strong selectivity for the decay of the  $\text{Xe}^{2+}$  states: e.g.,  $\text{Xe}^{2+} 1F_3$  decays preferably into  $\text{Xe}^{3+} 2P_{3/2}$  and  $2D_{5/2}$ , and  $\text{Xe}^{2+} 1P_1$  produces predominantly  $\text{Xe}^{3+} 2P_{3/2}$ .

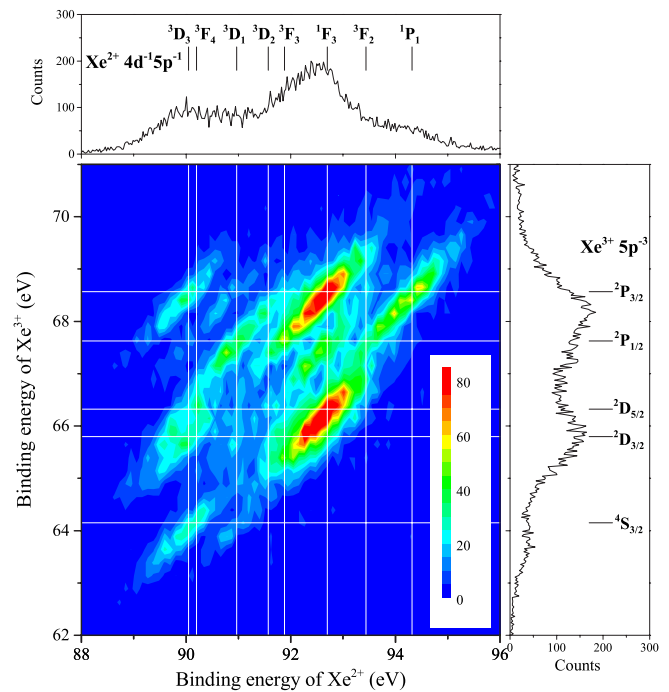


FIG. 4. (Color online) Yields of coincidences between two Auger electrons emitted from  $\text{Xe}^+ 4p^{-1}$ , as a function of binding energy of  $\text{Xe}^{2+}$  and that of  $\text{Xe}^{3+}$ , where level-to-level correlations on  $\text{Xe}^{2+} 4d^{-1}5p^{-1} \rightarrow \text{Xe}^{3+} 5p^{-3}$  are exhibited. The energy levels of the  $\text{Xe}^{2+}$  [12] and  $\text{Xe}^{3+}$  states [4,18] are indicated with horizontal and vertical lines, respectively. Coincidence yields are plotted on a linear scale. The top and right-hand panels show the projections of the coincidence yields onto the horizontal and vertical axes, respectively.

A sizable (34%) formation of  $\text{Xe}^{4+}$  in the “ $4p$ ” decay was found with a threshold electron-ion coincidence method [13]. In practice, we can find the corresponding events in the coincidence dataset, i.e., quadruple coincidences between a “ $4p$ ” photoelectron and three Auger electrons. Figure 5 shows the distribution of the sums of the four electrons’ kinetic energies. The curve exhibits peaks corresponding to the final  $\text{Xe}^{4+}$  states, on a background due to false coincidences. The probability of  $\text{Xe}^{4+}$  formation in the decay of “ $4p$ ”<sup>-1</sup> is estimated, from the true coincidence yields and from the detection efficiency, to be 9%. The present estimate indicates a less favorable  $\text{Xe}^{4+}$  formation, compared with the estimate made using a threshold electron-ion coincidence method [13]. While the relative energies of the  $\text{Xe}^{4+}$  levels have been precisely determined from the fluorescence lines of  $\text{Xe}^{4+}$  [19], the absolute values of the  $\text{Xe}^{4+}$  binding energies with respect to the neutral ground state are still uncertain. This is because there is a spread of values for the ionization energy of  $\text{Xe}^{3+}$  in the literature [20–22]. When we assume the  $\text{Xe}^{4+}$  threshold to be 106.3 eV, the  $\text{Xe}^{4+}$  peaks in Fig. 5 are well interpreted. The ionization energy of  $\text{Xe}^{3+}$  is therefore calculated to be 42.2 eV, when we take the  $\text{Xe}^{3+}$  threshold of  $64.09 \pm 0.04$  eV [4]. The value for the  $\text{Xe}^{3+}$  ionization energy agrees with the one reported by Emmons *et al.* [21].

Energy correlations among the three Auger electrons emitted in formation of the  $\text{Xe}^{4+} 5p^{-4}$  states are displayed in

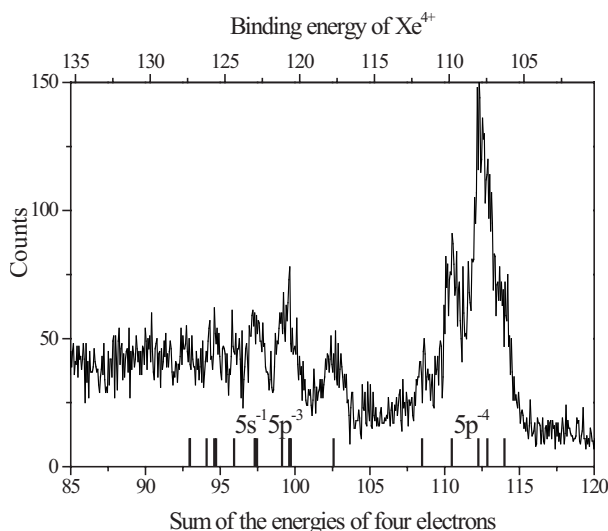


FIG. 5. Sum of the energies of four electrons in quadruple coincidences between a “ $4p$ ” photoelectron and three Auger electrons. The  $\text{Xe}^{4+}$  binding energies, attached on the top, are calculated with the kinetic energy sums and the photon energy (220.3 eV). The  $\text{Xe}^{4+}$  levels, derived from the relative energies of  $\text{Xe}^{4+}$  levels [19] and the present estimation of the  $\text{Xe}^{4+}$  threshold (106.3 eV), are indicated with bars.

Figs. 6(a) and 6(b), where coincidence yields are plotted as a function of fastest and middle Auger electrons’ energies [Fig. 6(a)] and that of fastest and slowest Auger electrons’ energies [Fig. 6(b)]. The energy distribution of the fastest Auger electrons, shown in Fig. 6(c), exhibits two broad maxima around 18 or 33 eV. The energy correlation maps in Figs. 6(a) and 6(b) represent clear coincidences among the fastest Auger electrons with around 33 eV and two other Auger electrons with less than 5 eV. The triple Auger electron emissions can be interpreted in terms of the process depicted in Fig. 2: the fastest Auger electrons are emitted by the Coster-Kronig transition from  $\text{Xe}^+ 4p^{n-1}$  to  $\text{Xe}^{2+} 4d^{-1}5s^{-1}$  satellites and that the two other Auger electrons result from the subsequent double Auger decay of these  $\text{Xe}^{2+}$  states to  $\text{Xe}^{4+} 5p^{-4}$ . Here, the decay of  $\text{Xe}^{2+} 4d^{-1}5s^{-1}$  satellites to  $\text{Xe}^{4+} 5p^{-4}$  can be stepwise via  $\text{Xe}^{3+}$  Rydberg states converging to excited  $\text{Xe}^{4+} 5p^{-4}$  states, though low statistics prevents the observation of discrete structures corresponding to intermediate states in the energy correlation maps. The probability of  $\text{Xe}^{4+}$  formation in the decay of  $\text{Xe}^{2+} 4d^{-1}5s^{-1}$  satellites is estimated to be 20%. Thus, this  $\text{Xe}^{4+}$  formation amounts to 3% in the decay of “ $4p^{n-1}$ ”, as added in Table II. Furthermore, the fastest Auger electrons with approximately 18 eV coincide with middle Auger electrons in the 10–18 eV range and with the slowest Auger electrons in the range 0–10 eV [see Figs. 6(a) and 6(b)]. Thus the triple Auger electron emissions are possibly assigned as double Auger decay of  $\text{Xe}^+ 4p^{n-1}$  to  $\text{Xe}^{3+} 4d^{-1} 5p^{-2}$  and the subsequent decay. In contrast to the  $\text{Xe}^{4+} 5p^{-4}$  formation, the three Auger electrons associated with the formation of  $\text{Xe}^{4+} 5s^{-1}5p^{-3}$  shows less clear energy correlations (not shown), and the corresponding process cannot be identified.

In conclusion, we have studied the whole nonradiative decay of  $\text{Xe}^+ 4p^{-1}$ , using a very efficient multielectron coin-

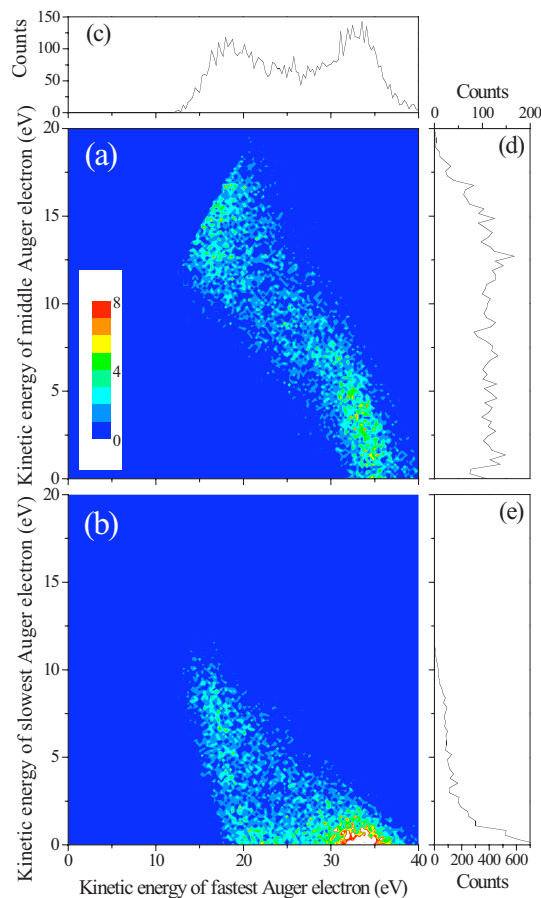


FIG. 6. (Color online) Energy correlation map among the three Auger electrons emitted on the formation of the  $\text{Xe}^{4+} 5p^{-4}$  states, plotted as (a) a function of fastest and middle Auger electrons’ energies and (b) that of fastest and slowest Auger electrons’ energies, and energy distribution curves of (c) the fastest, (d) middle, and (e) slowest Auger electrons. The binding energy range for the Auger final  $\text{Xe}^{4+}$  states is selected as 108–114.5 eV. Coincidence yields in (a) and (b) are plotted on a common linear scale. The energy correlation maps in (a) and (b) represent clear coincidences among the fastest Auger electrons with approximately 33 eV and two other Auger electrons with less than 5 eV.

idence method. We have observed the single, double, and triple Auger decay processes. The energy resolution of the present coincidence spectrometer makes it possible in most cases to resolve individual ionic levels relevant to the processes. The relative probability of each process has been determined from the coincidence yields. The present work demonstrates the great diagnostic power of the multielectron coincidence method for studying Auger decay mechanism.

#### ACKNOWLEDGMENTS

The authors are grateful to the Photon Factory staff for the stable operation of the PF ring. Financial support from JSPS and CNRS (PICS N-3407) are acknowledged. This work was performed under the approval of the Photon Factory Advisory Committee (Contracts Nos. 2004G210 and 2006G230).

- [1] J. Viefhaus, S. Cvejanovic, B. Langer, T. Lischke, G. Prümper, D. Rolles, A. V. Golovin, A. N. Grum-Grzhimailo, N. M. Kabachnik, and U. Becker, *Phys. Rev. Lett.* **92**, 083001 (2004).
- [2] J. Viefhaus, A. N. Grum-Grzhimailo, N. M. Kabachnik, and U. Becker, *J. Electron Spectrosc. Relat. Phenom.* **141**, 121 (2004).
- [3] J. Viefhaus, M. Braune, S. Korica, A. Reinköster, D. Rolles, and U. Becker, *J. Phys. B* **38**, 3885 (2005).
- [4] F. Penent, J. Palaudoux, P. Lablanquie, L. Andric, R. Feifel, and J. H. D. Eland, *Phys. Rev. Lett.* **95**, 083002 (2005).
- [5] Y. Hikosaka, T. Aoto, P. Lablanquie, F. Penent, E. Shigemasa, and K. Ito, *J. Phys. B* **39**, 3457 (2006).
- [6] P. Lablanquie, L. Andric, J. Palaudoux, U. Becker, M. Braune, J. Viefhaus, J. H. D. Eland, and F. Penent, *J. Electron Spectrosc. Relat. Phenom.* **156-158**, 51 (2007).
- [7] Y. Hikosaka, P. Lablanquie, F. Penent, T. Kaneyasu, E. Shigemasa, J. H. D. Eland, T. Aoto and K. Ito, *Phys. Rev. Lett.* **98**, 183002 (2007).
- [8] G. Wendin and M. Ohno, *Phys. Scr.* **14**, 148 (1976).
- [9] S. Svensson, N. Mårtensson, E. Basilier, P. Å. Malmquist, U. Gelius, and K. Siegbahn, *Phys. Scr.* **14**, 141 (1976).
- [10] S. Svensson, B. Eriksson, N. Mårtensson, G. Wendin, and U. Gelius, *J. Electron Spectrosc. Relat. Phenom.* **47**, 327 (1988).
- [11] S. Heinäsmäki, H. Aksela, J. Nikkinen, E. Kukkk, A. Kivimäki, S. Aksela, and S. Fritzsche, *J. Electron Spectrosc. Relat. Phenom.* **137-140**, 281 (2004).
- [12] A. Kivimäki, H. Aksela, J. Jauhiainen, M. Kivilompolo, E. Nömmiste, and S. Aksela, *J. Electron Spectrosc. Relat. Phenom.* **93**, 89 (1998).
- [13] T. Hayaishi, T. Matsui, H. Yoshii, A. Higurashi, E. Murakami, A. Yagishita, T. Aoto, T. Onuma, and Y. Morioka, *J. Phys. B* **35**, 141 (2002).
- [14] J. H. D. Eland, O. Vieuxmaire, T. Kinugawa, P. Lablanquie, R. I. Hall, and F. Penent, *Phys. Rev. Lett.* **90**, 053003 (2003).
- [15] Y. Hikosaka, T. Aoto, P. Lablanquie, F. Penent, E. Shigemasa, and K. Ito, *Phys. Rev. Lett.* **97**, 053003 (2006).
- [16] T. X. Carroll, J. D. Bozek, E. Kukkk, V. Myrseth, L. J. Sæthre, T. D. Thomas, and K. Wiesner, *J. Electron Spectrosc. Relat. Phenom.* **125**, 127 (2002).
- [17] J. M. Bizau and F. J. Wuilleumier, *J. Electron Spectrosc. Relat. Phenom.* **71**, 205 (1995).
- [18] J. G. Reyna Almandos, F. Bredice, M. Gallardo, C. J. B. Pagan, H. O. Di Rocco, and A. G. Trigueiros, *Phys. Rev. A* **43**, 6098 (1991).
- [19] E. B. Salomon, *J. Phys. Chem. Ref. Data* **33**, 765 (2004).
- [20] G. C. Rodrigues, P. Indelicato, J. P. Santos, P. Patté, and F. Parente, *At. Data Nucl. Data Tables* **86**, 117 (2004).
- [21] E. D. Emmons, A. Aguilar, M. F. Gharaibeh, S. W. J. Scully, R. A. Phaneuf, A. L. D. Kilcoyne, A. S. Schlachter, I. Álvarez, C. Cisneros, and G. Hinojosa, *Phys. Rev. A* **71**, 042704 (2005).
- [22] J. M. Bizau, C. Blancard, D. Cubaynes, F. Folkmann, J. P. Champeaux, J. L. Lemaire, and F. J. Wuilleumier, *Phys. Rev. A* **73**, 022718 (2006).